arXiv:1606.01859v1 [physics.atom-ph] 6 Jun 2016

# Gravitational wave detection with optical lattice atomic clocks

S. Kolkowitz*[,1], I. Pikovski[2,3], N. Langellier[2], M.D. Lukin[2], R.L. Walsworth[2,4], J. Ye†[,1]

[1] *JILA, NIST and University of Colorado, 440 UCB, Boulder, Colorado 80309, USA,*
[2] *Department of Physics, Harvard University, Cambridge, Massachusetts 02138, USA,*
[3] *ITAMP, Harvard-Smithsonian Center for Astrophysics, Cambridge, Massachusetts 02138, USA*
[4] *Harvard-Smithsonian Center for Astrophysics and Center for Brain Science, Cambridge, Massachusetts 02138, USA*

(Dated: June 7, 2016)

We propose a space-based gravitational wave detector consisting of two spatially separated, drag-free satellites sharing ultra-stable optical laser light over a single baseline. Each satellite contains an optical lattice atomic clock, which serves as a sensitive, narrowband detector of the local frequency of the shared laser light. A synchronized two-clock comparison between the satellites will be sensitive to the effective Doppler shifts induced by incident gravitational waves (GWs) at a level competitive with other proposed space-based GW detectors, while providing complementary features. The detected signal is a differential frequency shift of the shared laser light due to the relative velocity of the satellites, rather than a phase shift arising from the relative satellite positions, and the detection window can be tuned through the control sequence applied to the atoms' internal states. This scheme enables the detection of GWs from continuous, spectrally narrow sources, such as compact binary inspirals, with frequencies ranging from $\sim 3$ mHz - 10 Hz without loss of sensitivity, thereby bridging the detection gap between space-based and terrestrial GW detectors. Our proposed GW detector employs just two satellites, is compatible with integration with an optical interferometric detector, and requires only realistic improvements to existing ground-based clock and laser technologies.

The first direct detection of gravitational waves (GWs) by the Laser Interferometer Gravitational-Wave Observatory (LIGO) [1] heralds the dawn of a new era of astrophysics. The culmination of a century-long search [1–9], GW detection is now emerging as a new tool with which to study the universe, illuminating previously invisible astrophysical phenomena. In parallel, the developments of laser cooling and the laser frequency comb have given rise to optical atomic clocks with accuracies and stabilities at the $10^{-18}$ level [10–14]. As clock precision continues to improve, there is growing interest in the prospect of using optical atomic clocks for GW detection [9, 15, 16]. In this work we outline a proposal for a new GW detector composed of two spacecraft containing optical lattice atomic clocks linked over a single optical baseline. We analyze the prospects for GW detection and characterization using this scheme, including a comparison of the sensitivity of this technique to other proposed space-based detectors. We also highlight new and complementary GW measurement capabilities provided by space-based optical atomic clocks, and discuss the prospects for integrating our scheme with existing proposals.

While there is little doubt that LIGO and other terrestrial detectors will observe numerous additional GW events in the coming years, terrestrial detectors are only sensitive to GWs with frequencies above $\sim$10 Hz, due to seismic and Newtonian noise [1, 2, 17, 18]. The desire to observe a wider range of astrophysical phenomena over longer length and time scales has motivated proposals of larger scale, space-based GW detectors [15–22]. Though there are a wide variety of existing and proposed techniques[1–9], the proposals for future space-based GW detectors can be broadly classified in two categories. The first are optical interferometric detectors analogous to LIGO in space, such as the proposed Laser Interferometer Space Antenna (LISA) [17] and Evolved-LISA (eLISA) [18], which would be composed of three spacecraft forming either a two or three arm Michelson interferometer, with roughly equal length arms to reduce susceptibility to laser frequency noise. These GW detectors rely on large photon fluxes to split the optical interference fringe down to the required sensitivities, and detect signals in a broad frequency band determined by the detector arm length and residual acceleration noise of the satellites [17, 18].

The second class of proposed space-based GW detectors apply atomic physics techniques, such as atomic interferometry [19–22], and optical lattice atomic clocks, as described here. These atom-based detectors are sensitive to GWs in a similar and complementary manner to optical interferometers like LIGO and LISA, in that they also detect the changes in phase of an optical laser traveling between drag-free reference masses that are induced by the relative motion of the masses, as caused by the passing GW. However, in atom-based detectors the rate of phase change is measured locally at both ends of a single optical baseline by comparing the laser frequency to an atomic degree of freedom, with the atoms themselves serving as the reference masses. These detectors are therefore similar to the Doppler tracking method of GW detection [6–9, 16], in that they are sensitive to the relative velocities of the reference masses, rather than the

*shimonk@jila.colorado.edu
†ye@jila.colorado.edu

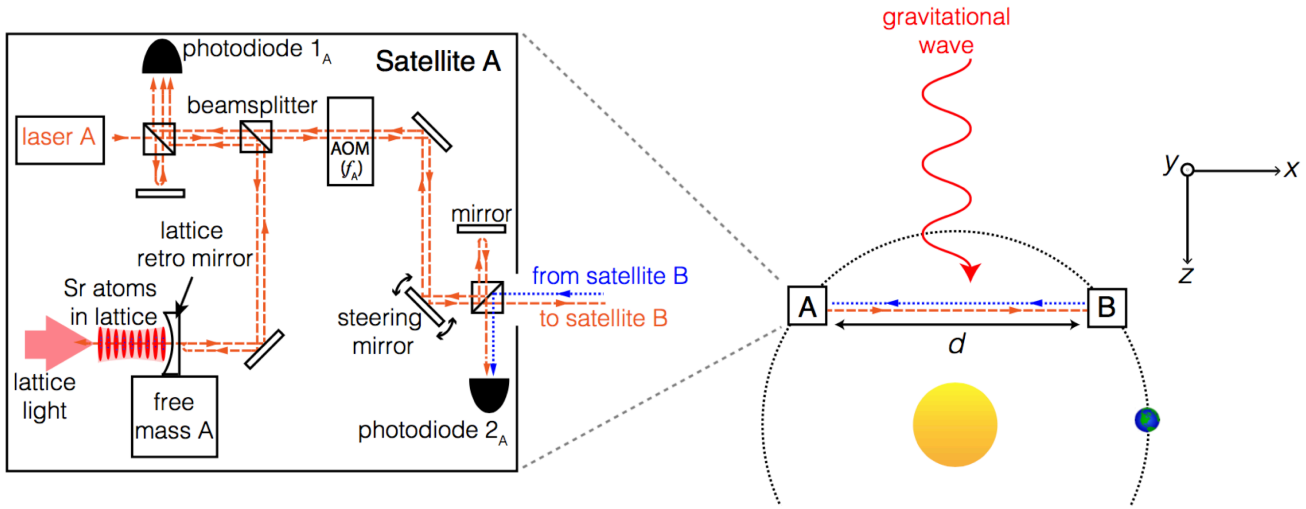



FIG. S1. **Proposed gravitational wave detector (not to scale).** Our detector consists of two identical drag-free satellites, A and B, separated from each other by a distance $d$ along the $x$-axis. Each satellite contains a free-floating reference mass, an ultra-stable laser, and a strontium optical lattice clock. A mirror is mounted on the free mass and is used to define the standing wave of light forming the optical lattice and confining the Sr atoms. Some of the laser light from satellite A (orange, dashed line) is sent to satellite B. The light first passes through an acousto-optic modulator (AOM) driven at frequency $f_A$, which offsets the frequency of the light reaching photodiode $2_B$ in satellite B and enables the phase locking of laser B to laser A through heterodyne detection. Vibrations and thermal drifts of the optics on each satellite can be corrected locally by feeding back on the beat notes at $2f_{A,B}$ on photodiodes $1_{A,B}$. Light from laser B (blue, dotted line) is sent back to satellite A to verify the phase lock, to maintain pointing stability, and to enable operation in the reverse mode, with laser A locked to laser B. A plus-polarized gravitational wave propagating along the $z$-axis induces relative motion between the two free masses (see supplemental materials), which can be detected using a clock comparison measurement protocol.

relative distance as in optical interferometers. By using the same laser light to synchronously probe the atoms on both ends of the baseline, laser frequency noise can be rejected without requiring a second optical arm, meaning atom-based proposals require only two spacecraft, not three. Furthermore, due to the high quality factor of atomic clock transitions, the optical power requirements on the link between satellites are more flexible than for optical interferometer GW detectors, as we discuss in detail below.

Atomic interferometer (AI) based proposals for GW detection use the motional degrees of freedom of the atoms to measure changes of the laser frequency, by using the reference laser light to spatially separate and then interfere two clouds of free ultracold atoms. In contrast, we propose to use an optical lattice clock to isolate the internal-state atomic clock transition from all external degrees of freedom, and to compare the reference laser frequency with the clock transition directly. This clock-based method has the advantage of relaxing the required atomic temperatures, from picoKelvin for AI to microKelvin for clocks.

Our proposed detector also offers complementary features to optical interferometer based GW detectors. Dynamical decoupling (DD) control sequences applied to the internal states of the atoms [23, 24] can extend the range of GW frequencies to which our detector can be maximally sensitive, from milliHertz to tens of Hertz, providing a tunable, narrowband GW detector for tracking spectrally narrow but evolving GW sources such as inspiraling black hole or neutron star binaries, and bridging the spectral gap between space-borne and terrestrial optical interferometric detectors [1, 2, 17, 18]. Furthermore, quantum techniques such as atomic spin-squeezing and entangled states [25–27] offer the potential for future improvements in sensitivity, detection bandwidth, and spectral range. Finally, because optical atomic clocks are currently the most accurate frequency references [10–14], and can provide improved sensitivity to beyond-Standard-Model phenomena that may couple to atomic properties such as mass, charge, and spin [28–30], there is already considerable motivation to develop space-hardy optical clocks, and to integrate them with other proposed GW detectors.

*Sensing GWs using optical lattice atomic clocks.*—Our proposed GW detector, illustrated in Fig. 1, consists of two drag-free satellites in heliocentric orbit (A and B), separated by a length $d$ and connected over a single optical link using conventional optical telescopes. Each satellite contains its own optical lattice atomic clock [10–12], and its own ultra-stable laser [31]. The laser in satellite B is kept phase locked to the light sent from satellite A over the optical link, such that the two lasers function as a single ultra-stable clock laser shared between the two satellites. In each satellite the lattice confining the clock atoms is created using the standing wave formed

by retro-reflecting a magic wavelength laser [10–12] off of a mirror mounted on a free-floating reference mass, such that the atoms are strongly confined in the reference frame of the free mass and are therefore in free-fall, despite their confinement. Drag-free masses have been studied in great detail by the LISA collaboration, and this technology is currently undergoing testing and verification in the LISA Pathfinder space mission [32]. The phase of the clock lasers in each satellite is kept referenced to the same mirror using interferometry [33] to cancel out any relative motion of the lasers or optics with respect to the atoms. To cancel the radiation pressure exerted on the free mass by the lattice and clock beams, a set of equal power, counter-propagating lasers are incident on the opposite sides of the free masses. For a 1 kg mass and a 1 W lattice beam, the remaining acceleration noise from the quantum radiation pressure shot noise of the lattice, clock, and compensation beams is far below the GW detector noise floor at frequencies of interest [34].

Operation of the GW detector consists of a synchronous comparison between the two optical lattice atomic clocks. The frequency of laser A is compared to the clock transition in the atoms in satellite A using Ramsey spectroscopy. Synchronization signals are transmitted to satellite B, so that an identical Ramsey measurement is performed on the atoms in satellite B using laser B, which is phase locked to laser A. Both Ramsey measurements are performed with the same interrogation time $T$. The Ramsey phases accumulated by the atoms in each satellite are recorded, and can then be compared over a standard communication channel. Because the satellites effectively share a single laser and the two measurements are offset by the time required for the laser light to travel from A to B, any laser frequency noise will be common mode for the two measurements, resulting in the same additional acquired phase in each clock, and will thus be rejected. This method of laser frequency noise rejection has been previously utilized in optical atomic clocks to cancel laser noise arising from the Dick effect, and thereby achieve the quantum projection noise limit [35–37]; it has also been proposed for use in AI-based GW detectors [20].

A passing plus-polarized GW of strain amplitude $h$ and frequency $f_{\rm GW}$, propagating along the $z$-axis perpendicular to the optical link between the satellites, will induce relative motion between the free masses A and B, and therefore an effective Doppler shift of the reference clock light sent from satellite A to B. Hence the atoms in satellite B will experience a local oscillator of a different optical frequency than the atoms in satellite A, and will accumulate a different Ramsey phase. When the two clocks are compared, they will appear to have "ticked" at different rates, with the maximum fractional frequency difference between the two clocks given by

$$s \equiv \frac{\delta\nu}{\nu} = h\left|\sin\left(\pi f_{\rm GW} d/c\right)\right|, \tag{1}$$

where $c$ is the speed of light (see supplemental materials for derivation). Note that $s = h$ for the optimal clock spacing $d = \lambda_{\rm GW}/2$, where $\lambda_{\rm GW} = c/f_{\rm GW}$ is the GW wavelength. When compared to an optical interferometric GW detector such as LISA [17, 18], with total optimized arm length $d$, the fractional frequency difference $s$ between two optimally spaced clocks will be equivalent to the fractional change in differential arm length experienced by the optical interferometer. However, at GW frequencies other than the optimal frequency the magnitude of the detectable signal is determined by the detector's transfer function $\mathcal{T}(f)$ [38], which has a different scaling for a clock-based GW detector than for an optical interferometer [9] (see supplemental materials).

The transfer function $\mathcal{T}_\phi(f)$ for optical interferometric GW detectors such as LISA, which measure a differential phase shift of the laser light rather than a frequency shift, is frequency independent for GW frequencies below $c/2d$, but scales as $\mathcal{T}_\phi(f) \propto 1/f_{\rm GW}$ at higher frequencies where the photon transit time is longer than a half period of the GW [17, 18]. Therefore, because the 1 mHz - 1 Hz frequency range is of primary interest for space-based detectors [17–20], $\mathcal{T}_\phi(f)$ sets a maximum arm length for an optical interferometer on the order of $\sim 1\times10^9$ meters. In contrast, because the clock GW detector compares the local laser frequency at the two satellites, and is thus only sensitive to the relative velocity of the satellites, the transfer function $\mathcal{T}_c(f)$ of the clock GW detector scales as $\mathcal{T}_c(f) \propto f_{\rm GW}$ for $f_{\rm GW} < c/2d$, but is frequency independent at higher frequencies [9, 39]. We therefore propose a clock GW detector with a baseline length $d = 5\times10^{10}$ m, setting the minimum frequency that can be detected at the detector's peak sensitivity to be $c/2d \approx 3$ mHz. Note that a LISA-like baseline length of $5\times10^9$ meters could be used without sacrificing sensitivity at GW frequencies above ∼30 mHz.

*Expected sensitivity.*—To compare the optical lattice clock method to other existing and proposed GW detectors, we begin by considering the quantum noise limits to the sensitivity of the clock technique. We consider two clocks separated by a distance $d$, sharing a clock laser over the optical link with a laser linewidth $\Delta_L$, which is limited by current optical cavity technology to be at least an order of magnitude broader than the natural atomic line width $\Delta_A$ [23, 31]. We assume that the clocks are atom projection noise limited, and that there is perfect single shot readout of each atom's final internal state following the Ramsey sequence. As the two clocks effectively share a single clock laser, laser noise is common mode and the Ramsey free precession time $T$ can be extended considerably beyond the laser coherence time [35–37]. Here we assume $T$ can be pushed out to the radiative lifetime of the clock transition, $T_{max} = 1/(2\pi\Delta_A)$. Note that reaching $T_{max}$ also requires the suppression of atomic interactions to avoid collisional broadening and many-body losses, which can be accomplished by loading the atoms into a 3D optical lattice with one atom per site. In addition we assume that the atom lifetime in the lattice exceeds $T_{max}$. Thus for $N$ atoms in each clock and a

series of optimized Ramsey measurements, each with precession time $T_{max}$, and a total measurement time $\tau$, the smallest detectable fractional frequency difference $\sigma_{min}$ between the two clocks, and hence the smallest measurable GW-induced strain with our scheme, is given by

$$\sigma_{min}(\tau) = \frac{\delta\nu_{min}}{\nu}\bigg|_{\tau} = \frac{\sqrt{\Delta_A}}{\nu\sqrt{2\pi\tau N}}, \tag{2}$$

where $\nu$ is the frequency of the optical clock transition [40]. To analyze the achievable GW sensitivity using this technique, we consider a next-generation strontium-87 optical lattice clock, as $^{87}$Sr has the narrowest demonstrated clock transition linewidth [10, 40]. The $^{87}$Sr $^1S_0 - ^3P_0$ clock transition is at $\nu = 430$ THz, and the transition linewidth is $\Delta_A = 1$ mHz, yielding $T_{max} = 160$ s [41]. Current work is experimenting with the loading of $10^4 - 10^5$ $^{87}$Sr atoms from a degenerate Fermi gas into a 3D optical lattice [42] to achieve record-long coherence times. With improved lattice power and engineering, one may expect a strontium optical lattice clock to operate with $\sim 1 \times 10^7$ atoms. Taking $N = 7 \times 10^6$ atoms yields a minimum detectable fractional frequency difference of $\sigma_{min} = 1.1 \times 10^{-20}/\sqrt{\text{Hz}}$. Although this represents a 4 order of magnitude improvement over the demonstrated stability [13], the anticipated large improvements in the atom number and coherence time, along with improved laser and correlated noise spectroscopy, will help realize this gain. Note that because $\sigma_{min}$ can only be achieved using measurements with optimal Ramsey precession time $T_{max} = 160$ s, our detector is spectrally narrowband and thus is not well suited for the detection of short burst GWs. Nonetheless, as we discuss below, our detector should be well suited for the detection of GWs emanating from continuous, spectrally narrow sources, such as compact binary inspirals.

*Detector noise floor and dynamical decoupling sequences.*—At low frequencies the detector noise floor will be dominated by residual acceleration noise of the free reference masses. This noise has been carefully analyzed by the LISA collaboration [17, 18, 32], and a $1/f^2$ scaling of the noise is anticipated up to a frequency cutoff of $\sim$3 mHz, which when combined with the clock GW detector transfer function $\mathcal{T}_c(f)$ gives a low frequency scaling of noise-limited strain sensitivity with $1/f^3$. At higher frequencies atom projection noise dominates, which for fixed $T$ is frequency independent. However, optimal sensitivity, $s = \sigma_{min}$, is achievable using a Ramsey sequence only if half the period of the GW is longer than or equal to $T_{max}$, as shown in panel 1 of Fig. 2a. As illustrated in panel 2 of Fig. 2a, the signal from higher frequency GWs will partially average out over the course of a single Ramsey measurement of length $T_{max}$, giving rise to reduced sensitivity at higher frequencies. In order to search for GWs of frequency $f_{\rm GW} > 1/2T_{max}$, a Ramsey interrogation time of $T' = 1/2f_{\rm GW}$ can be used (panel 3 of Fig. 2a). This results in a reduction in GW sensitivity for all frequencies $f_{\rm GW} \geq 1/2T_{max}$ by a factor of $\sqrt{T'/T_{max}}$, due to increased atom projection noise from the shorter Ramsey measurements. Therefore the strain sensitivity envelope for optimally chosen Ramsey sequences at each $f_{\rm GW}$ scales as $\sqrt{f}$ at high frequencies, as shown by the dashed orange line in Fig. 2b and c.

Fortunately, quantum metrology techniques can be applied to achieve optimal, frequency-independent GW sensitivity at higher frequencies. As illustrated in panel 4 of Fig. 2a, by using a dynamical decoupling (DD) sequence consisting of a Ramsey sequence combined with a train of periodically spaced $\pi$-pulses matched to the frequency of the GW [23, 24], it is possible to remain sensitive to a GW with frequency $f_{\rm GW} > 1/2T_{max}$ while still interrogating for $T_{max}$, such that the sensitivity is still given by Eq. 2 in a narrow frequency band around $f_{\rm GW}$. Assuming high-fidelity $\pi$-pulses can be performed, the optimal GW sensitivity $\sigma_{min}$ can be reached for frequencies up to the Rabi frequency for the clock transition, which for conservative local clock laser intensities can exceed $\Omega_{max} \approx 100$ Hz. Utilizing DD sequences with $\sim 3 \times 10^3$ $\pi$-pulses or fewer, it is therefore possible to remain maximally sensitivity to GWs with frequencies up to $\sim 10$ Hz. These DD sequences are similar in spirit to the "signal recycling" cavity that is used in the LIGO GW detector to enhance sensitivity in a tunable narrow bandwidth [2, 43]; however such a recycling scheme is impossible for a much longer baseline space-based optical interferometer like LISA due to optical diffraction. We note that similar "resonant" pulse sequences have also been recently proposed for use in AI detectors [44]. The broad frequency range over which our proposed clock GW detector can be tuned and remain maximally sensitive is well suited for the study of binary inspirals and mergers, which chirp upward in frequency as the two bodies spiral inwards at an increasing rate [1]. Once an on-going GW event has been detected, the spacing of the $\pi$-pulses in the DD detection sequence can be "chirped" along with the signal to remain optimally sensitive to the particular event throughout its evolution.

*Comparison to other proposals.*—In Fig. 2b and 2c we plot a comparison of the strain sensitivities of the clock GW detector and the proposed LISA mission [17, 18], using Ramsey and DD sequences respectively. The LISA GW detectors use optical interferometry, a proven concept for which extensive design and testing have already been performed. Furthermore, the LISA GW detectors will provide broadband sensitivity as plotted in Fig. 2b, in contrast to our clock GW detector, which makes a narrowband measurement at a frequency selected by the applied control sequence. We therefore consider our proposal as complementary to the LISA mission; we envision that an optical clock GW detector could be integrated with, and operated in parallel to, a LISA optical interferometer without reducing the sensitivity of either GW detector. As an example of the advantages of such a hybrid detector, following the detection of an on-going binary inspiral at mHz frequencies by LISA, the clock GW detector would enable continued observation of the event as the frequency rises out of the detection band-

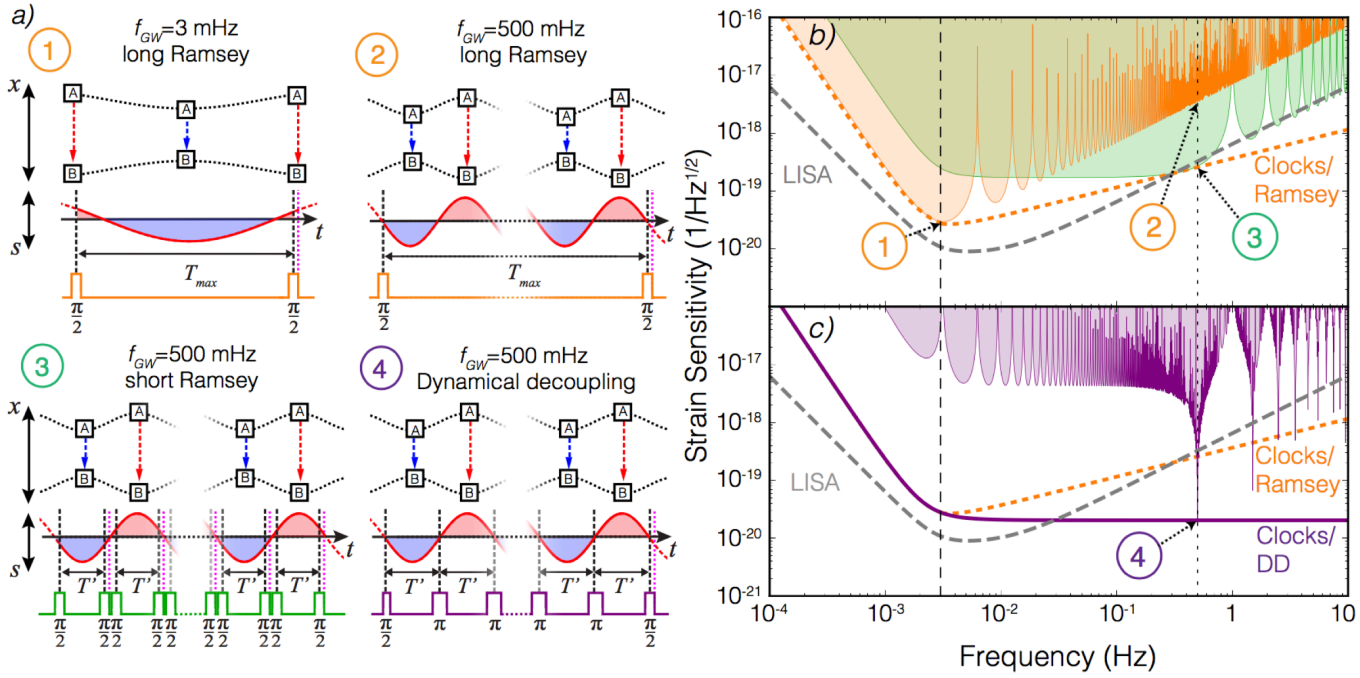



FIG. S2. **Measurement protocols and comparison of gravitational wave sensitivities.** ***a)*** *(1)* A Ramsey pulse sequence performed on the atomic clock transition can be used to detect a GW with $f_{\rm GW} = 3$ mHz, for which a half period matches the atomic linewidth limited interrogation time $T_{max} = 160$ s. From top to bottom, we depict the effect of a GW on the relative position of the two satellites (A and B), the sign of the Doppler shift induced on the transmitted laser light, the accumulated clock signal $s$ (see Eq. 1), and the pulse sequence (pink dotted line indicates atom state readout). *(2)* The same Ramsey pulse sequence as in panel 1 will measure a reduced signal for a GW of frequency $f_{\rm GW} = 500$ mHz, because the fast Doppler shift oscillations will average out. *(3)* A series of shorter Ramsey sequences with $T' = 1$ s can be used to detect a $f_{\rm GW} = 500$ mHz GW, with reduced sensitivity due to the increase in atom projection noise. *(4)* A DD sequence with 159 periodic $\pi$-pulses separated by $T' = 1$ s can instead be employed to detect a GW with $f_{\rm GW} = 500$ mHz, resulting in the same total accumulated signal $s$ as the Ramsey measurement for $f_{\rm GW} = 3$ mHz as shown in panel 1. ***b)*** Noise-limited strain sensitivity of our detector to a monochromatic GW using a Ramsey sequence with interrogation time $T_{max} = 160$ s (orange filled region), and a Ramsey sequence with $T' = 1$ s (green filled region). The Ramsey sensitivity envelope for optimized Ramsey sequences at each GW frequency is shown (orange dotted line), and the projected strain sensitivity of LISA is plotted for comparison [17]. The clock GW detector consists of one clock per satellite, each with $7 \times 10^6$ atoms, with the baseline length optimized for $f_{\rm GW} \geq 3$ mHz, giving $d = 5 \times 10^{10}$ m. ***c)*** Noise-limited strain sensitivity of our detector to a monochromatic GW using a DD sequence with 159 periodic $\pi$-pulses with total interrogation time $T_{max} = 160$ s (purple filled region), and the DD sensitivity envelope for optimized DD sequences at each GW frequency (thick purple line). In both Fig. 2b and 2c the strain sensitivities corresponding to panels 1-4 in Fig. 2a are highlighted. The clock GW detector has narrow regions of reduced sensitivity for each measurement sequence when the time between pulses, $(T_{max}, T')$, is an integer multiple of a GW period. The polarization and direction of propagation of a GW can also change the measurable signal for LISA and the clock GW detector (see supplemental materials).

width of LISA, all the way through the final moments of the merger, or until it becomes detectable by terrestrial GW detectors. In addition, LISA could greatly benefit if next-generation optical lattice atomic clocks are made ready for space, as the ultra-stable lasers locked to the clocks would provide the best possible local oscillator for the optical interferometer.

Atomic interferometer (AI) GW detectors have been proposed with comparable predicted sensitivities to both LISA and our optical atomic clock proposal, for similar baseline lengths, and requiring only two satellites [19, 20]. Importantly, the atoms in an AI GW detector are completely unconfined, and hence there is no need for drag-free reference masses as the atoms themselves are in free-fall. However, the AI proposal also requires that the atoms be cooled to picoKelvin temperatures [45], as the measurement is made using the motional states of the atoms. In contrast, our clock-based scheme requires drag-free satellite technology, but this enables the loading of atoms at microKelvin temperatures into the ground state of the optical lattice [10]. Furthermore, the radiative lifetime limited sensitivity of the clock detector is also a strict bound on the sensitivity of an AI GW detector using the same atomic species and atom number [19].

*Analysis of optical power requirements.*—In the preceding analysis we assumed that the sensitivity of our optical atomic clock GW detector was limited by atom pro-

jection noise at frequencies above 3 mHz, with all other sources of noise being significantly smaller. In particular, photon shot noise is a considerable fraction of the noise budget of other space-based GW detector proposals [18]. However, in the case of the optical clock detector, as with other Doppler shift GW detectors, photon shot noise is less restrictive [9]. Specifically, photon shot noise enters the clock GW detector through noise on the phase-locked loop (PLL) used to lock laser B to the light arriving from laser A, with the phase error variance of the loop given by

$$\delta\phi^2 \approx \frac{h\nu B}{\eta P_B} + \frac{\Delta_L}{B}, \tag{3}$$

where $P_B$ is the power from laser A that is received at satellite B, $\eta$ is the detector quantum efficiency, $\Delta_L$ is the linewidth of each laser, and $B$ is the PLL bandwidth [46]. The first term results from photon shot noise on the optical link, while the second term arises from phase excursions of laser B due to the finite loop bandwidth. To keep lasers A and B coherent at all times the PLL must not undergo phase cycle slips, requiring $\delta\phi^2 \ll 1$. In this limit the relevant phase noise spectrum will be entirely white. An additional requirement is that the optimal loop bandwidth $B_{opt}$, found by minimizing $\delta\phi^2$, must be larger than the gravitational wave frequency to be detected so that the loop can respond to the GW signal. In the limit of long measurement time relative to the optimal loop bandwidth, $B_{opt}\tau \gg 1$, the noise floor due to both atom projection noise and photon shot noise is then given by (see supplemental materials for derivation),

$$\sigma^2(\tau) = \frac{1}{(2\pi\nu)^2 T\tau}\left(\frac{1}{N} + \frac{T}{\tau}\sqrt{\frac{h\nu\Delta_L}{\eta P}}\right). \tag{4}$$

Because the photon shot noise (second term) in Eq. 4 scales with $1/\tau^2$, a well known result for Doppler shift GW searches [9], while the atom projection noise term scales as $1/\tau$, the atom projection noise will always dominate over photon shot noise at sufficiently long averaging times, and hence Eq. 4 will reduce to Eq. 2 when $T = T_{max}$. Note that this requires the phase coherence time of a candidate GW to be longer than the total averaging time $\tau$ required to reach the atom projection noise limit. If the clock GW detector sensitivity were to be improved by increasing the atom number, the full gain in sensitivity could be realized by either increasing the optical power in order to reach the lower projection noise floor in the same averaging time, or by simply averaging for longer.

Taking the laser A and B linewidths each to be 1 Hz [31], the detector efficiency to be $\eta = 0.5$, the maximum desired detectable GW frequency to be 10 Hz, and the required GW coherence time to be at most 1 day, we find that the received optical power at satellite B must exceed $P_B \approx 95$ pW. At 1 day of averaging, the minimum detectable strain of a continuous GW with a frequency between 3 mHz and 10 Hz would then be $h_{min} \approx 3.7\times10^{-23}$. For long optical baselines, the power received at satellite B is related to the power transmitted from satellite A by $P_B = P_A\left(\pi r^2\nu/dc\right)^2$, where $r$ is the radius of the telescope used on both satellites [38]. Hence for $r = 30$ cm and the proposed satellite separation of $d = 5\times10^{10}$ m (see Fig. 2), the clock GW detector requires a transmitted power of $P_A \approx 1.4$ W, comparable to the $\sim$1 W of transmitted power required by the LISA detector [17, 18].

*Sources of future improvement.*—While our proposal already offers competitive sensitivities in a complementary frequency range to other proposed space-based GW detectors, there are also potential upgrades that can be anticipated to further improve detector performance. For example, a clock network composed of a distributed array of spacecraft with phase coherent optical links between nearest neighbors could enable clocks in space to be compared over considerably longer distances than a single baseline scheme, and could also provide optimal sensitivity for arbitrarily polarized GWs propagating in any direction, as well as the ability to localize the GW source direction. In addition, as ground-based optical atomic clocks become increasingly precise there is growing motivation to build space-based clocks for metrology, in order to avoid the gravitational redshifts caused by seismic activity [40, 47]. We emphasize that our GW detection scheme is compatible with a space-based clock network designed primarily for time-keeping and navigation.

We can also anticipate increases in the detection bandwidth without sacrificing sensitivity by using spin-squeezed and GHZ atomic states [25–27]. These entangled quantum states can be used to bypass the standard quantum limit for short interrogation times, and hence change the sensitivity scaling with atom number from $\sigma_{min} \propto 1/\sqrt{N}$, as given in Eq. 2, to $\sigma_{min} \propto 1/N$. To mitigate the photon shot noise restrictions at short averaging times, more sophisticated allocations of the atomic resources using phase estimation protocols could also be employed [27]. Furthermore, in the present proposal we focused exclusively on the 1 mHz linewidth, $^1S_0 - ^3P_0$ transition in $^{87}$Sr. The use of correlated noise spectroscopy offers the prospect of switching to a different isotope or atomic species with a narrower clock transition, thereby increasing the coherent interrogation time and improving the sensitivity to GWs [48, 49]. Candidate atoms include neutral Mg [50], or the bosonic isotopes $^{84}$Sr and $^{88}$Sr, where the linewidth of the otherwise forbidden clock transition can potentially be controlled using a second dressing laser [51].

*Outlook.*—We have proposed a gravitational wave (GW) detector consisting of two satellites each containing an optical lattice atomic clocks linked by ultra-stable optical laser light over a single baseline. Synchronous clock comparisons will allow detection of GWs via the effective Doppler shift of the shared laser light. With realistic pro-

jections for the atomic clock performance, our detector is expected to provide comparable strain sensitivity to that of other proposed space-based GW detectors based on optical and atomic interferometers [17–20], along with several complementary features. In particular, our detector bridges the detection gap between space-based and terrestrial GW detectors through tunable, narrowband GW detection with constant sensitivity over a broad frequency range from ∼3 mHz to 10 Hz, while also offering flexible laser power requirements for the spacecraft link, and more readily realizable atomic technology. Beyond GW detection, clocks also offer sensitivity to other fundamental physical and astronomical phenomena that may couple to atomic properties such as mass, charge, and spin, including searches for dark matter, violations of fundamental symmetries, and variations of fundamental constants [28–30]. Key challenges to be addressed in future works include: the development of optimized clock measurement protocols tailored for GW sources of interest, as well as spectral characterization and detection feasibility studies of known GW sources; the design of space-hardy, high-precision atomic clocks and ultrastable lasers, which will also directly benefit other proposed space-based GW detectors; and the demonstration of quantum metrology techniques involving entanglement to enhance both the sensitivity and detection bandwidth of clock GW detectors.

*Acknowledgements.*—We thank Avi Loeb and Dan Maoz for providing the initial inspiration to pursue this work. We also thank Johannes Borregaard, Akihisa Goban, Jason Hogan, Mark Kasevich, Edward Marti, Holger Müller, and Dan Stamper-Kurn for helpful discussions and insights. This work was supported in part by NIST, NASA, JILA PFC, NSF, CUA, NSSEFF, DARPA, and the NSF through a grant to ITAMP. S.K. thanks the NRC postdoctoral fellowship program for support.

[1] B. P. Abbott, R. Abbott, T. D. Abbott, M. R. Abernathy, F. Acernese, K. Ackley, C. Adams, T. Adams, P. Addesso, R. X. Adhikari, *et al.* (LIGO Scientific Collaboration and Virgo Collaboration), Phys. Rev. Lett. **116**, 061102 (2016).
[2] B. Abbott, R. Abbott, R. Adhikari, P. Ajith, B. Allen, G. Allen, R. Amin, S. Anderson, W. Anderson, M. Arain, *et al.*, Reports on Progress in Physics **72**, 076901 (2009).
[3] K. Ishidoshiro, M. Ando, A. Takamori, H. Takahashi, K. Okada, N. Matsumoto, W. Kokuyama, N. Kanda, Y. Aso, and K. Tsubono, Phys. Rev. Lett. **106**, 161101 (2011).
[4] M. Coughlin and J. Harms, Phys. Rev. Lett. **112**, 101102 (2014).
[5] S. Detweiler, The Astrophysical Journal **234**, 1100 (1979).
[6] S. Aoyama, R. Tazai, and K. Ichiki, Phys. Rev. D **89**, 067101 (2014).
[7] B. Bertotti, R. Ambrosini, J. Armstrong, S. Asmar, G. Comoretto, G. Giampieri, L. Iess, Y. Koyama, A. Messeri, A. Vecchio, *et al.*, Astronomy and Astrophysics **296**, 13 (1995).
[8] A. Konopliv, S. Asmar, E. Carranza, W. Sjogren, and D. Yuan, Icarus **150**, 1 (2001).
[9] J. W. Armstrong, Living Rev. Relativity **9**, E2 (2006).
[10] B. J. Bloom, T. L. Nicholson, J. R. Williams, S. L. Campbell, M. Bishof, X. Zhang, W. Zhang, S. L. Bromley, and J. Ye, Nature **506**, 71 (2014).
[11] N. Hinkley, J. A. Sherman, N. B. Phillips, M. Schioppo, N. D. Lemke, K. Beloy, M. Pizzocaro, C. W. Oates, and A. D. Ludlow, Science **341**, 1215 (2013).
[12] I. Ushijima, M. Takamoto, M. Das, T. Ohkubo, and H. Katori, Nature Photonics **9**, 185 (2015).
[13] T. Nicholson, S. Campbell, R. Hutson, G. Marti, B. Bloom, R. McNally, W. Zhang, M. Barrett, M. Safronova, G. Strouse, *et al.*, Nature Comm. **6** (2015).
[14] N. Huntemann, C. Sanner, B. Lipphardt, C. Tamm, and E. Peik, Physical review letters **116**, 063001 (2016).
[15] A. Loeb and D. Maoz, arXiv preprint arXiv:1501.00996 (2015), arXiv:1501.00996.
[16] A. Vutha, New Journal of Physics **17**, 063030 (2015).
[17] K. Danzmann, T. Prince, P. Binetruy, P. Bender, S. Buchman, J. Centrella, M. Cerdonio, N. Cornish, A. Cruise, C. Cutler, *et al.*, Assessment Study Report ESA/SRE **3**, 2 (2011).
[18] P. Amaro-Seoane, S. Aoudia, S. Babak, P. Binétruy, E. Berti, A. Bohe, C. Caprini, M. Colpi, N. J. Cornish, K. Danzmann, *et al.*, Classical and Quantum Gravity **29**, 124016 (2012).
[19] P. W. Graham, J. M. Hogan, M. A. Kasevich, and S. Rajendran, Phys. Rev. Lett. **110**, 171102 (2013).
[20] J. M. Hogan and M. A. Kasevich, arXiv preprint arXiv:1501.06797 (2015).
[21] N. Yu and M. Tinto, General Relativity and Gravitation **43**, 1943 (2011).
[22] S.-W. Chiow, J. Williams, and N. Yu, Phys. Rev. A **92**, 063613 (2015).
[23] M. Bishof, X. Zhang, M. J. Martin, and J. Ye, Phys. Rev. Lett. **111**, 093604 (2013).
[24] J. Taylor, P. Cappellaro, L. Childress, L. Jiang, D. Budker, P. Hemmer, A. Yacoby, R. Walsworth, and M. Lukin, Nature Physics **4**, 810 (2008).
[25] I. D. Leroux, M. H. Schleier-Smith, and V. Vuletić, Phys. Rev. Lett. **104**, 073602 (2010).
[26] J. G. Bohnet, K. C. Cox, M. A. Norcia, J. M. Weiner, Z. Chen, and J. K. Thompson, Nature Photonics **8**, 731 (2014).
[27] M. Kessler, E., P. Komar, M. Bishof, L. Jiang, S. Sorensen, A., J. Ye, and D. Lukin, M., Phys. Rev. Lett. **112**, 190403 (2014).
[28] A. Derevianko and M. Pospelov, Nature Physics **10**, 933 (2014).
[29] A. Arvanitaki, J. Huang, and K. Van Tilburg, Physical Review D **91**, 015015 (2015).
[30] C. Delaunay and Y. Soreq, arXiv preprint arXiv:1602.04838 (2016).
[31] T. Kessler, C. Hagemann, C. Grebing, T. Legero, U. Sterr, F. Riehle, M. J. Martin, L. Chen, and J. Ye, Nature Photonics **6**, 687 (2012).
[32] P. McNamara, S. Vitale, K. Danzmann, L. P. S. W.

Team, *et al.*, Classical and Quantum Gravity **25**, 114034 (2008).
[33] S. M. Foreman, A. D. Ludlow, M. H. de Miranda, J. E. Stalnaker, S. A. Diddams, and J. Ye, Phys. Rev. Lett. **99**, 153601 (2007).
[34] G. Heinzel, V. Wand, A. Garcia, O. Jennrich, C. Braxmaier, D. Robertson, K. Middleton, D. Hoyland, A. Rüdiger, R. Schilling, *et al.*, Classical and Quantum Gravity **21**, S581 (2004).
[35] C. W. Chou, D. B. Hume, J. C. J. Koelemeij, D. J. Wineland, and T. Rosenband, Phys. Rev. Lett. **104**, 070802 (2010).
[36] M. Takamoto, T. Takano, and H. Katori, Nature Photonics **5**, 288 (2011).
[37] T. Nicholson, M. Martin, J. Williams, B. Bloom, M. Bishof, M. Swallows, S. Campbell, and J. Ye, Phys. Rev. Lett. **109**, 230801 (2012).
[38] S. L. Larson, W. A. Hiscock, and R. W. Hellings, Physical Review D **62**, 062001 (2000).
[39] Where here we have set aside the "blind-spot" frequencies, present for all optical GW detecters, that occur when $\lambda_{\rm GW} = d$.
[40] A. D. Ludlow, M. M. Boyd, J. Ye, E. Peik, and P. O. Schmidt, Reviews of Modern Physics **87**, 637 (2015).
[41] M. M. Boyd, T. Zelevinsky, A. D. Ludlow, S. M. Foreman, S. Blatt, T. Ido, and J. Ye, Science **314**, 1430 (2006).
[42] S. L. Campbell *et al.*, "Ten second atom-light coherence in a quantum degenerate 3d optical lattice clock," (2016), in preparation.
[43] B. J. Meers, Physical Review D **38**, 2317 (1988).
[44] P. W. Graham, J. M. Hogan, M. A. Kasevich, and S. Rajendran, "A resonant mode for gravitational wave detectors based on atom interferometry," (2016), to be submitted.
[45] T. Kovachy, J. M. Hogan, A. Sugarbaker, S. M. Dickerson, C. A. Donnelly, C. Overstreet, and M. A. Kasevich, Phys. Rev. Lett. **114**, 143004 (2015).
[46] L. G. Kazovsky, Lightwave Technology, Journal of **4**, 182 (1986).
[47] C. W. Chou, D. B. Hume, T. Rosenband, and D. J. Wineland, Science **329**, 1630 (2010).
[48] T. Rosenband and D. Leibrandt, arXiv preprint arXiv:1303.6357 (2013).
[49] P. Komar, E. M. Kessler, M. Bishof, L. Jiang, A. S. Sorensen, J. Ye, and M. D. Lukin, Nature Physics **10**, 582 (2014).
[50] A. Kulosa, D. Fim, K. Zipfel, S. Rühmann, S. Sauer, N. Jha, K. Gibble, W. Ertmer, E. Rasel, M. Safronova, *et al.*, Phys. Rev. Lett. **115**, 240801 (2015).
[51] R. Santra, E. Arimondo, T. Ido, C. H. Greene, and J. Ye, Phys. Rev. Lett. **94**, 173002 (2005).

arXiv:1606.01859v1 [physics.atom-ph] 6 Jun 2016

# Supplemental material for "GW detection with optical lattice atomic clocks"

S. Kolkowitz, I. Pikovski, N. Langellier, M.D. Lukin, R.L. Walsworth, J. Ye

(Dated: June 7, 2016)

## I. DERIVATION OF THE EFFECTIVE DOPPLER SHIFT INDUCED BY A PASSING GRAVITATIONAL WAVE

A passing gravitational wave (GW) induces periodic changes in the light travel time between emitter and detector[1]. In this section we derive the magnitude of this effect as a function of the GW amplitude, the orientation between the satellites and the direction of propagation of the GW, and the distance between the clocks. Similar analyses have been performed for proposed detectors that utilize Doppler tracking [1] and pulsar timing [2]. Our detection scheme involves only a one-way link as in the case of pulsar timing, but with full experimental control on both sites for the emission and detection of the signal.

Weak gravitational fields are captured by a perturbed metric $g_{\mu\nu} = \eta_{\mu\nu} + h_{\mu\nu}$, where $\eta_{\mu\nu}$ is the Minkowski metric and $|h_{\mu\nu}| \ll 1$ is a small perturbation. GWs are described in the transverse traceless gauge by the metric:

$$g_{\mu\nu} = \begin{pmatrix} -1 & 0 & 0 & 0 \\ 0 & 1+h_+ & h_\times & 0 \\ 0 & h_\times & 1-h_+ & 0 \\ 0 & 0 & 0 & 1 \end{pmatrix}, \tag{S1}$$

where $h_+(t-z/c)$ and $h_\times(t-z/c)$ correspond to the two polarizations of the wave, which travels in the $z$-direction.

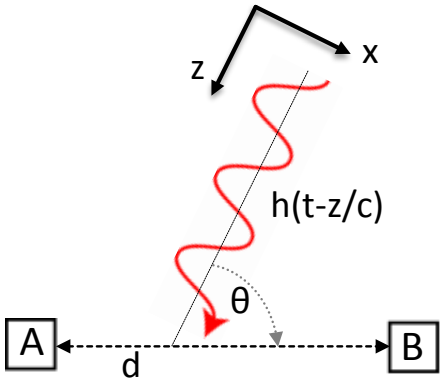



FIG. S1. A GW incident along the $z$-axis periodically changes the light travel distance between $A$ and $B$.

[1] One can expect an additional effect due to the time dilation induced by the GW itself. However, this effect would be of second order in GW strain amplitude $h$, and is therefore vanishingly small when compared to the sensitivity of current clocks.

For simplicity we calculate the effect for a plus-polarized plane wave with $h = h_+ = |h|e^{-i2\pi f(t-z/c)}$, where $f$ is the frequency of the wave and $|h|$ its amplitude (for arbitrary polarization angles $\psi$, the final result remains valid with the substitution $|h| \to |h_+|\cos(2\psi) + |h_\times|\sin(2\psi)$). The line element for this metric is then

$$ds^2 = -c^2dt^2 + (1+h)dx^2 + (1-h)dy^2 + dz^2. \tag{S2}$$

We now consider the situation depicted in Fig. S1, where a light signal is sent at time $t$ from system $A$ to system $B$, which is at a distance $d$ in the $x-z$-plane. A light-like curve is defined by $ds^2 = 0$. Parameterizing the curve by $r$ with $x = r\sin\theta$, $y = 0$ and $z = r\cos\theta$, the coordinates for the curve become (to lowest order in $h$):

$$cdt = \left(1 + \frac{1}{2}h\sin^2\theta\right)dr. \tag{S3}$$

As the signal is emitted at coordinate time $t$ and travels from $A$ to $B$ in a time $t_1 = t + d/c$ to lowest order in $h$, it travels an apparent distance

$$D_{AB} = c\int_t^{t_1} dt' = \int_0^d \left(1 + \frac{1}{2}h(1-\cos^2\theta)\right)dr, \tag{S4}$$

where the GW is parameterized by $h = h(t + r/c - r\cos\theta/c)$. In terms of its indefinite integral H(t), the above expression becomes

$$D_{AB} = c(t_1 - t) = d + \frac{c}{4\pi f}\times \\ \times(1+\cos\theta)\left[H(t) - H\left(t + \frac{d}{c}(1-\cos\theta)\right)\right]. \tag{S5}$$

In flat space the distance traveled by the light would just be given by $d$, but the presence of the GW periodically changes the apparent length of the light path. In Doppler tracking techniques, the signal is reflected back to $A$ and measured there. Here, instead, we consider measurement directly on $B$. The rate of change gives a Doppler shift of the signal $\sigma \equiv \dot{D}_{AB}/c = \Delta\nu/\nu$, where $\nu$ is the optical frequency:

$$s = \frac{\Delta\nu}{\nu} = \frac{1+\cos\theta}{2}\left[h(t) - h\left(t + \frac{d}{c}(1-\cos\theta)\right)\right]. \tag{S6}$$

This apparent Doppler shift is the signal to be detected at $B$. The effect is maximized for $\theta = \pi/2$, i.e. for the detector aligned perpendicularly to the GW, while the signal disappears for $\theta = 0$, i.e. in the direction of propagation of the GW. Similarly to interferometric detection

schemes, the frequency shift is due to transversal motion of test bodies as the GW is passing.

From equation (S6), we can see that when using a single shared local oscillator to compare two clocks positioned a distance $d$ apart in the plane ($\theta = \pi/2$) of a passing GW of amplitude $|h|$ and wavelength $\lambda_{\rm GW} = c/f$, the clocks will appear to "tick" at different rates, with the maximum fractional frequency difference between the two clocks given by

$$s_{max} = |h| \left| \sin\left(\pi \frac{d}{\lambda_{\rm GW}}\right) \right|. \tag{S7}$$

Note that the detector is insensitive to GWs with wavelengths that match a multiple of the baseline $d$.

## II. DETECTOR SENSITIVITY

For space-based detectors, the effect of geometric factors on the sensitivity is typically described by the transfer function $\mathcal{T}(f)$, which captures the detector response to specific GW frequencies [3]. We can express Eq. (S6) in Fourier-space, which gives

$$\tilde{s}(f) = \frac{1}{2}\tilde{h}(f)\left(1 - e^{i2\pi f d/c}\right), \tag{S8}$$

where the tilde denotes the Fourier transform $\tilde{s}(f) = \int dt e^{i2\pi f t} s(t)$. The expression multiplying $\tilde{h}$ in Eq. (S8) depends only on the geometry of the detector and gives rise to its geometric transfer function, which is $\mathcal{T}_c(f) = |(1 - e^{i2\pi f d/c})/2|^2 = \sin^2(\pi f d/c)$. It is different than for the case of interferometric detectors in two ways: we consider only a single one-way link between two satellites and are sensitive to frequency, i.e. changes in the phase of the light rather than the phase itself. For optical interferometric detectors sensitive to phase, the additional derivative results in the transfer function $\mathcal{T}_\phi(f) = \mathrm{sinc}^2(\pi f d/c)$ [4]. A comparison between the transfer functions of a phase and a frequency detector for an otherwise identical geometry is shown in Fig. S2.

The actual measured signal for the clock-based detector depends on the measurement scheme used for the atoms. A long integration time $T$ increases the sensitivity (see Eq. 2 in the main text), but is limited by the atomic linewidth. The signal acquired for a clock measurement between $t_0$ and $t_0 + T$ is therefore

$$\bar{s} = \frac{1}{T}\int_{t_0}^{T+t_0} dt s(t) = \int_{-\infty}^{\infty} dt F(t - t_0) s(t), \tag{S9}$$

where $F(t)$ is a window function that captures the measurement sequence of duration $T$. For a Ramsey measurement (ignoring the finite pulse durations), the window function is just $F(t) = 1/T$ for $t \in [t_0, t_+T]$ and $F(t) = 0$ otherwise. For a continuous GW with $h(t) = |h|\sin(2\pi f t + \varphi)$, this gives

$$\bar{s} = \frac{|h|}{\pi f T}\left|\sin\left(\pi f \frac{d}{c}\right)\sin(\pi f T) \times \right. \\ \left. \times \cos\left(\pi f\left(2t_0 + \frac{d}{c} + T\right) + \varphi\right)\right|. \tag{S10}$$

As we consider a continuous signal, we can adapt the starting time of the measurement to account for $\varphi$ and thus set the argument of the cosine to 0 to give

$$\bar{s} = |h|\left|\sin\left(\pi f \frac{d}{c}\right)\,\mathrm{sinc}(\pi f T)\right|. \tag{S11}$$

The sine term in Eq. (S11) captures the light-travel time between the two satellites, while the sinc-function appears due to intergation for a time $T$. Equivalently, we can describe the measurement by a transfer function $\mathcal{T}_T(f) = \mathcal{T}_c(f)\mathrm{sinc}^2(\pi f T)$. Ideal sensitivity is achieved only for the frequency $f = 1/(2T)$ and distance $d = cT$. For higher frequency GWs, the signal strength is reduced due to the finite integration time $T$. Reducing the integration time to $T' < T$ gives an ideal signal at $2fT' = 1$, but causes the atomic clocks to be less sensitive due to atom projection noise.

Using dynamical decoupling allows the detector to be ideally sensitive at frequencies other than $1/(2T)$. Instead of the integrated signal given in Eq. (S9), the detection is performed with a window function $F_{dd}(t)$, such that

$$\bar{s}_{dd} = \left|\int_{-\infty}^{\infty} dt s(t) F_{dd}(t - t_0)\right|. \tag{S12}$$

The window function is defined by the particular dynamical decoupling sequence that is utilized. For our

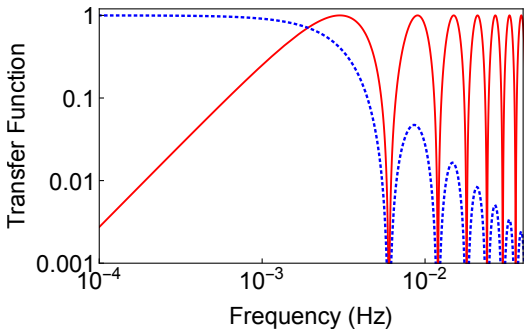



FIG. S2. Transfer functions for a detector sensitive to changes in frequency, $\mathcal{T}_c(f)$ (red curve), as compared to a detector sensitive to phase, $\mathcal{T}_\phi(f)$ (blue dotted curve). Frequency measurements yield the maximal signal for $f = (n + 1/2)c/d$, $n \in \mathbb{N}_0$, while the sensitivity is drastically reduced for $f < c/(2d)$. In contrast, phase measurements become significantly less sensitive for frequencies $f \gtrsim c/(2d)$, even without the presence of noise. Here the distance between satellites is $d = 5 \times 10^{10}$ m, as in the main text.

purposes, we use the PDD sequence with $n$ $\pi$-pulses, given by $TF_{dd}(t) = \Theta(t) + 2\sum_{k=1}^{n}(-1)^k\Theta(t - kT/n) + (-1)^{n+1}\Theta(t - T)$, where $\Theta(x)$ is the Heaviside step function. Adapting the measurement time such that $\varphi + \pi f d/c = \pi/2$, the signal becomes

$$\bar{s}_{dd} = |h| \left| \sin\left(\pi f \frac{d}{c}\right) \operatorname{sinc}\left(\pi f \frac{T}{n}\right) \times \right. \\ \left. \times \frac{1}{n}\sum_{k=1}^{n}(-1)^{k+1}\sin\left(\pi f(2k-1)\frac{T}{n}\right)\right|. \tag{S13}$$

With DD, the signal is maximized for $f = n/(2T)$, but is reduced for other frequencies. Thus DD is ideal to select a specific frequency at which the detector is maximally sensitive. The minima closest to the main peak occur at $f = (n \pm 1)/(2T)$, we thus define the detector bandwidth as $\Delta f \approx 1/T$. Outside this frequency range the detector can still operate, but with a reduced sensitivity.

Restoring the angular dependence as in Eq. (S6), and averaging over all angles and polarizations, we get

$$\bar{s}_{dd} = |\langle h\rangle| \left| \sqrt{\frac{2}{3} - \frac{1}{(2\pi f d/c)^2} + \frac{\sin(4\pi f d/c)}{2(2\pi f d/c)^3}} \operatorname{sinc}\left(\pi f \frac{T}{n}\right) \times \right. \\ \left. \times \frac{1}{n}\sum_{k=1}^{n}(-1)^{k+1}\sin\left(\pi f(2k-1)\frac{T}{n}\right)\right|, \tag{S14}$$

where $\langle h\rangle = \sqrt{|h_\times|^2 + |h_+|^2}/\sqrt{2}$ is the mean GW amplitude.

## III. DERIVATION OF OPTICAL POWER REQUIREMENTS

Our proposed detector utilizes a phase-locked loop (PLL) to lock laser B in satellite B to the light sent from laser A in satellite A, such that the two lasers function as a single ultra-stable clock laser shared between the two satellites. Such a setup allows for correlated noise spectroscopy [5–7]. Here we analyze the power requirements stemming from the laser linewidth and the shot noise in the PLL. The fractional relative frequency between Laser A and B is $y = \delta\nu/\nu$, and we denote the uncertainty in the relative frequency as

$$\sigma_\nu^2 = \langle \bar{\delta\nu}^2\rangle/\nu^2, \tag{S15}$$

where $\bar{\delta\nu} = (1/\tau)\int_{t_0}^{t_0+\tau}\delta\nu(t)dt$ is the average relative frequency in a measurement window of time $\tau$. The above expression is the true variance of the average frequency, in practice the Allan variance (or two-sample variance) is a more practical measure of the frequency instability [8]. With a window function $F(t)$, which captures the measurement for a duration $\tau$, we can write Eq. (S15) as

$$\sigma_\nu^2 = \langle\left(\int_{-\infty}^{\infty} dt F(t-t_0)y(t)\right)^2\rangle \\ = \int_0^\infty df|\tilde{F}(f)|^2 S_y(f), \tag{S16}$$

where we expressed the variance in terms of the one-sided power spectral density (PSD) $S_y(f)$ and the transfer function of the measurement, given by the Fourier transform of the window function $\tilde{F}(f) = \int dt e^{i2\pi f t}F(t)$. For subsequent Ramsey measurements without any dead time, the measurement corresponds to an overall window of duration $\tau$ with the transfer function $|\tilde{F}(f)|^2 = \operatorname{sinc}^2(\pi f\tau)$. In this case, the above expression becomes

$$\sigma_\nu^2 = \frac{1}{\tau^2\nu^2\pi^2}\int_0^\infty df \sin^2(\pi f\tau)S_\varphi(f), \tag{S17}$$

where $S_\varphi(f) = \nu^2 S_y(f)/f^2$ is the PSD for relative phase noise[2]. For white frequency noise, as is typical for a single free-running laser, we have $S_y(f) = \Delta_L/\nu^2$ and the deviation becomes $\sqrt{\sigma_\nu^2} = \sqrt{\Delta_L/(\tau\nu^2)} \propto \tau^{-1/2}$, with the same scaling with $\tau$ as atom projection noise. However, because we use synchronous detection to cancel the laser noise, we are only concerned with the relative phase noise between laser A and laser B. With the PLL engaged, the relative phase noise is white within the loop bandwidth $B$, and the Allan deviation instead scales with $1/\tau$ [9]. Therefore, after a sufficiently long averaging time, the white phase noise of the light is always subdominant to atom projection noise.

To illustrate this, we use a simple PLL model which captures the main features (for a detailed analysis of phase-locked loops and various loop designs, see Refs. [10, 11]). We assume that the laser phase $\phi^B$ is updated in a time step $t_k$ according to $\phi^B_{k+1} = \phi^B_k + \phi^{corr}_k$, where $\phi^{corr}_k$ is an applied correction based on the outcome of the heterodyne measurement of lasers $A$ and $B$. The demodulated outcome is a signal $i \propto \sin(\phi^A - \phi^B)$ with a shot noise contribution $n$. For small phase differences $\delta\phi = \phi^A - \phi^B$ and a loop bandwidth $B$, the correction in the loop is $\phi^{corr}_k = B\int_{t_k}^{t_k+1/B}\delta\phi_k + n(t_k)$. Without shot noise, this loop would give $\phi^B_{k+1} \to \phi^A_k$ in the limit of arbitrarily large bandwidth. However, the shot noise restricts the bandwidth, as it increases with larger $B$. For times

[2] One can also derive the two-sample variance (or Allan variance) $\sigma_y^2 = \langle(\bar{y_1} - \bar{y_2})^2\rangle/2$ for two subsequent measurement cycles of duration $\tau$, which is typically used in characterizing clock stability instead of the true variance. A similar calculation as above gives the Allan variance $\sigma_y^2 = \langle(\int dt\bar{y}(t)(F(t-t_1) - F(t-t_2))^2\rangle/2 = \int_0^\infty df\, 2\sin^2(\pi f\tau)|\tilde{F}(f)|^2 S_y(f)$. For the case of Ramsey measurements with no dead time, this gives $\sigma_y^2 = \int_0^\infty df S_y(f) 2\sin^4(\pi f\tau)/(\pi f\tau)^2$. For white phase noise the Allan variance is larger than the true variance by a factor 3/2 [8].

$t \gg 1/B$, we can treat the steps as infinitesimal and obtain a loop differential equation $\dot{\delta\phi} = -B\delta\phi - \nu + Bn(t)$, where $\nu$ is the laser frequency. Writing this in Fourier space, we obtain the noise power spectral density

$$S_\varphi(f) = \frac{\Delta_L}{(2\pi f)^2 + B^2} + \frac{h\nu B^2}{\eta P_B((2\pi f)^2 + B^2)}, \quad \text{(S18)}$$

where $B$ is the loop bandwidth, $\Delta_L$ is the linewidth of the two lasers, $P_B$ is the received power from satellite A at the PLL photodetector, and $\eta$ is the detection efficiency. The first term is due to white frequency noise from the two laser linewidths, which is suppressed in the PLL within the bandwidth $B$, while the second term is the photon shot noise of the optical link, which sets the noise floor for the heterodyne detection in the PLL. This PSD follows from our simple model, but captures the main noise features of the phase-locked loop, namely a phase noise filter up to the bandwidth $B$, with an additional shot noise contribution from heterodyne detection in the loop [10]. Using this PSD in the integral in Eq. (S17) to get the noise contribution from the relative laser phase gives $\int_0^\infty df \sin^2(\pi f\tau)/((2\pi f)^2 + B^2) = (1 - e^{-B\tau})/(8B)$. Including the atom projection noise given in the main text, the overall variance in frequency measurement is therefore

$$\sigma^2 = \frac{1}{(2\pi\nu)^2 T\tau}\left(\frac{1}{N} + \frac{1 - e^{-B\tau}}{2\tau/T}\left(\frac{\Delta_L}{B} + \frac{h\nu}{\eta P_B}B\right)\right). \quad \text{(S19)}$$

The bandwidth of the loop can be optimized to minimize the additional phase noise, which gives $B = \sqrt{\eta P_B \Delta_L/(h\nu)}$. For optimized loop bandwidth and in the limit $B\tau \gg 1$, the above expression becomes

$$\sigma^2 = \frac{1}{(2\pi\nu)^2 T\tau}\left(\frac{1}{N} + \frac{T}{\tau}\sqrt{\frac{h\nu\Delta_L}{\eta P_B}}\right). \quad \text{(S20)}$$

The contribution from the laser phase noise therefore averages down faster than the atom projection noise (see Fig. S3). For sufficiently large number of runs $\tau/T$, the sensitivity will always be limited by atom projection noise. We note that for read-out sequences other than Ramsey, Eq. (S16) still holds and can be computed for an arbitrary window function. However, the read-out sequence does not affect the scaling given in Eq. (S19), which depends only on a sufficiently large bandwidth of the PLL.

To reach the atom projection noise limit, the laser noise needs to be averaged down for a sufficiently long time $\tau_{av}$. From Eq. (S20) we can find an estimate for this averaging time:

$$\tau_{av} > \frac{N}{2\pi\Delta_A}\sqrt{\frac{h\nu\Delta_L}{\eta P_B}}, \quad \text{(S21)}$$

where we have set $T = T_{max} = 1/2\pi\Delta_A$.

For the parameters used in the main text, we get $\tau_{av} = 1$ day for $P_B = 95$ pW. A lower power is acceptable if the averaging time is allowed to be longer (also, an optimized PLL design could potentially improve the requirements compared to the simple model used here). In practice, however, this averaging time may be limited by other noise sources, in which case increased transmitted laser power, a shorter satellite distance, or a narrower laser linewidth are beneficial. The scalings of fractional frequency instability with $\tau$ for various laser powers and atomic linewidths are shown in Fig. S3.

The averaging time will be fundamentally limited by the duration of the GW at the specific frequency of interest. Compact binary inspirals produce continuous GWs which experience a chirp towards higher frequencies, given by [12]:

$$\dot{f} = \frac{96}{5}\pi\left(\frac{\pi G M_c}{c^3}\right)^{5/3} f^{11/3}, \quad \text{(S22)}$$

where $G$ is the gravitational constant and $M_c = (m_1 m_2)^{3/5}/(m_1 + m_2)^{1/5}$ is the effective chirp mass of a binary system with masses $m_1$ and $m_2$. The number of GW cycles in a time $t \in [t_1, t_2]$ small compared to the GW period is $dn_{cyc} = f dt$, or $n_{cyc} = \int_{f_1}^{f_2} df f/\dot{f}$. Assuming $f_2 - f_1 \approx 1/T_{max}$, we find that the time the GW is within this frequency range is given by

$$\tau_{\rm GW} = \frac{n_{cyc}}{f} \approx 2.5 \times 10^{10}\text{s}\left(\frac{10\text{mHz}}{f}\right)^{8/3}\left(\frac{2.6 M_\odot}{M_c}\right)^{5/3}, \quad \text{(S23)}$$

where $M_\odot = 2 \times 10^{30}$ kg is the solar mass, and we have normalized $M_c$ to the mass value for an inspiral of two objects with $m_1 = m_2 = 3M_\odot$. For such

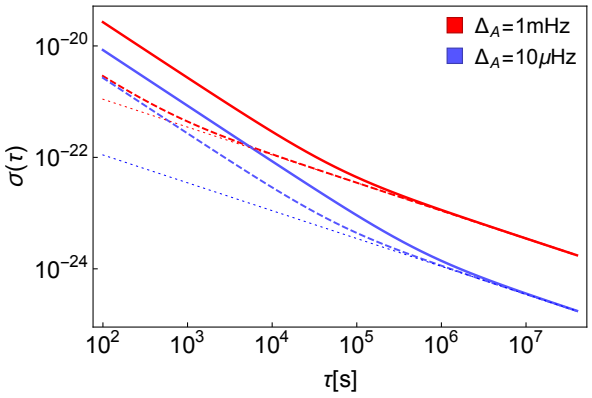



FIG. S3. Fractional frequency instability as a function of averaging time $\tau$ as given in Eq. (S20). The red curves correspond to an atomic linewidth $\Delta_A = 1$ mHz as in the main text, while the blue curves are for a narrower atomic transition with $\Delta_A = 10\mu$Hz. The thick and dashed lines differ by the received optical power: 95 pW (red thick line), 10 nW (blue thick line) and 1$\mu$W (blue and red dashed lines). The dotted lines show the atom projection noise limit as given in Eq. 2 of the main text. For short averaging times photon shot noise dominates and the noise scales with $1/\tau$, while at long averaging times atom projection noise dominates and the noise scales as $1/\sqrt{\tau}$.

sources, and for frequencies in the ∼10 mHz range, the GW has an essentially fixed frequency over hundreds of years. For heavier sources, however, $\tau_{\rm GW}$ can be much shorter; for a black hole binary as detected by LIGO ($m_1 = 36M_\odot, m_2 = 29M_\odot$) we have $\tau_{\rm GW} \approx 15$ years in the above frequency range around $f = 10$ mHz. For optimal GW detection, we require $\tau_{av} < \tau_{\rm GW}$, which is reasonable for most sources expected in the frequency range of interest. We also note that this is not a strict limitation for a source with a known frequency chirp, as the measurement sequence can be easily adapted to chirp the detection window along with the source.


[1] F. B. Estabrook and H. D. Wahlquist, General Relativity and Gravitation **6**, 439 (1975).
[2] S. Detweiler, The Astrophysical Journal **234**, 1100 (1979).
[3] N. J. Cornish and L. J. Rubbo, Physical Review D **67**, 022001 (2003).
[4] R. Schilling, Classical and Quantum Gravity **14**, 1513 (1997).
[5] C. W. Chou, D. B. Hume, J. C. J. Koelemeij, D. J. Wineland, and T. Rosenband, Phys. Rev. Lett. **104**, 070802 (2010).
[6] M. Takamoto, T. Takano, and H. Katori, Nature Photonics **5**, 288 (2011).
[7] T. Nicholson, M. Martin, J. Williams, B. Bloom, M. Bishof, M. Swallows, S. Campbell, and J. Ye, Phys. Rev. Lett. **109**, 230801 (2012).
[8] J. Rutman, Proceedings of the IEEE **66**, 1048 (1978).
[9] J. W. Armstrong, Living Rev. Relativity **9**, E2 (2006).
[10] L. G. Kazovsky, J. Lightwave Technol. **4**, 182 (1986).
[11] C. C. Chen and C. S. Gardner, NASA STI/Recon Technical Report N **87** (1987).
[12] M. Maggiore, *Gravitational waves* (Oxford Univ. Press, 2008).